RSC Advances

PAPER

View Article Online
View Journal | View Issue

Cite this: *RSC Adv.*, 2017, **7**, 30191

Hydroxyapatite/N-doped carbon dots/Ag_3PO_4 composite for improved visible-light photocatalytic performance

Q. Chang, †*[a] X. Meng,†[a] S. L. Hu, *[a] F. Zhang[b] and J. L. Yang[ac]

In this study, a new hydroxyapatite/N-doped carbon dots/Ag_3PO_4 (HA/N-CDs/Ag_3PO_4) composite was prepared by a facile hydrothermal approach and *in situ* ion-exchange reaction method. The photocatalytic performance of the as-prepared samples was investigated by the degradation of methylene blue (MB) under visible light irradiation. It was found that the HA/N-CDs/Ag_3PO_4 composite exhibited much higher photocatalytic activity and stability compared with HA/N-CDs and HA/Ag_3PO_4. In addition, the effect of the amount of silver loading on the photocatalytic activity of the composite was evaluated. The experimental results showed that a higher silver loading amount led to a decrease of both the UV-Vis absorption and photocatalytic performance. A suitable content of silver loading produced the highest photocatalytic activity. The substantial improvement in the photocatalytic performance of the composite can be attributed to the synergetic effects of HA support, CDs and the formed Ag_3PO_4, which led to an increase of active sites, suppression of the electron–hole recombination, and the stability improvement of Ag_3PO_4. The HA/N-CDs/Ag_3PO_4 photocatalyst synthesized *via* a cost-effective route is a promising candidate in organics removal.

Received 1st May 2017
Accepted 5th June 2017

DOI: 10.1039/c7ra04881e

rsc.li/rsc-advances

1. Introduction

Photocatalysis has been considered to be a potential technology to solve environmental and energy problems by using solar light,[1,2] thus receiving considerable attention. During the past decades, numerous photocatalysts have been developed.[3–8] However, the variety of visible-light photocatalysts is still limited. Therefore, to develop efficient photocatalysts is critically important.

Hydroxyapatite (HA) is well-known as an inorganic biomaterial due to its excellent bioactivity and biocompatibility.[9] In recent years, it has also been demonstrated to display remarkable properties as a catalyst support, since it possesses very unique properties, including rich polar groups (OH^-, PO_4^{3-}), good affinity, high stability and low cost. For instance, the composites of metal (Ru, Au, Co) supported on HA[10,11] and semiconductor loaded on HA,[12–15] have been prepared and found to exhibit enhanced catalytic performance.

Carbon dots (CDs), a novel nanocarbon material, have drawn intensive interest due to their excellent properties, such as low cost, low toxicity, easy functionalization and so on.[16,17] Given their electron-accepting/transfer properties, CDs have been proven to be a potential photocatalyst.[18–20] Meanwhile, it has been demonstrated that introducing CDs into semiconductors could remarkably enhance the photocatalytic activities of the composites.[21–25] The tunable photocatalytic properties of CDs have also been widely investigated in our research group.[26–31] More recently, the present authors developed a hydroxyapatite supported N-doped CDs composite to solve the aggregation and non-recyclability of CDs.[32] However, the high photocatalytic efficiency and visible light utilization still remain a challenge. It is necessary to develop new and efficient photocatalysts.

Ag_3PO_4, as one of the semiconductor photocatalysts, has been reported to show excellent photocatalytic activity.[33] However, owing to the solubility and unstable property under light irradiation,[34,35] plus the consumption of noble metal, the photocatalytic application of Ag_3PO_4 is strongly limited. To solve the limitations of Ag_3PO_4, hybrid photocatalysts have been proposed.[13,14,22,36–40] Among them, Zhang *et al.*[22] reported that coupling Ag_3PO_4 with CDs was an effective strategy to improve the stability of Ag_3PO_4, since the dissolution of Ag_3PO_4 could be impeded by CDs. Hong *et al.*[13] and Chai *et al.*[14] also pointed out hydroxyapatite supported Ag_3PO_4 prepared *via in situ* ion-exchange method could effectively reduce the cost and improve the photocatalytic activity of the composite. Considering the unique characteristics of CDs and HA, coupling them

[a]*School of Materials Science and Engineering, North University of China, Xueyuan Road 3, Taiyuan 030051, China. E-mail: changneu@gmail.com; hsliang@yeah.net; Fax: +86 351 3559638; Tel: +86 351 3559638*

[b]*Jinzhong Institute of Quality and Technical Supervision Inspection & Measurement, Yuci 030600, China*

[c]*State Key Laboratory of New Ceramics and Fine Processing, Tsinghua University, Beijing 100084, China*

† These authors contributed equally.

with Ag_3PO_4 to form a ternary HA/CDs/Ag_3PO_4 composite is expected to improve both the photocatalytic efficiency and stability, as well as reduce the cost. The purpose of this investigation was, therefore, to synthesize HA/N-CDs/Ag_3PO_4 composite in an attempt to develop a new hybrid photocatalyst with improved photocatalytic efficiency and stability *via* a cost-effective route, evaluate the microstructure and photocatalytic performance of the composites, and identify the underlying mechanisms.

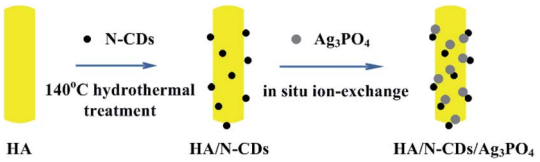

Fig. 1 Schematic illustration of the synthesized process of HA/N-CDs/Ag_3PO_4.

2. Experimental

2.1 Materials preparation

2.1.1 Materials. All chemicals were of analytical grade, purchased from Sinopharm Chemical Reagent Co. Ltd. (Shanghai, China) and used without further purification.

2.1.2 Synthesis of N-CDs. N-CDs were synthesized through a hydrothermal method using ethylene glycol and ammonia as carbon and amine source. Typically, 25 mL ethylene glycol was transferred into a Teflon-lined autoclave. The autoclave was sealed and kept at 200 °C for 5 h. After cooling to room temperature, the CDs solution was obtained. Then 10 mL of CDs was mixed with 536 μL of ammonia solution. The mixture was then transferred to the Teflon-lined autoclave again and heated at 200 °C for 5 h. After cooling to room temperature, N-CDs were obtained.

2.1.3 Synthesis of HA powders. HA powders were also prepared *via* the hydrothermal method by reacting $CaCl_2$ with $Na_2HPO_4 \cdot 12H_2O$. Briefly, the calcium solution and phosphate solution were prepared separately. The phosphate solution at a Ca/P molar ratio of 1.67 was added drop-wise to the calcium solution at room temperature. A proper amount of NaOH solution was added during the process to adjust the pH value to 11. The mixture was then transferred to the Teflon-lined autoclave and heated at 150 °C for 15 h. After the autoclave cooled to room temperature, the sediment was separated by centrifuging and washed by distilled water and ethanol several times. The resulting sludge was dried at 80 °C to obtain the final HA.

2.1.4 Synthesis of HA/N-CDs. HA/N-CDs composite was fabricated *via* the procedure reported previously.[32]

2.1.5 Synthesis of HA/N-CDs/Ag_3PO_4. The HA/N-CDs/Ag_3PO_4 composite was synthesized by *in situ* ion-exchange method. First, $AgNO_3$ crystals were dissolved in distilled water to obtain aqueous solution. The obtained HA/N-CDs powders were then added to $AgNO_3$ aqueous solution. The mixed solution was vigorously stirred for 4 h under dark condition. The resulting heterostructured HA/N-CDs/Ag_3PO_4 composites were separated by centrifuging and washed by distilled water three times. After dried at 60 °C for 12 h in a vacuum oven, the final HA/N-CDs/Ag_3PO_4 powders were obtained. To obtain the optimal silver loading amount, a series of samples with different theoretical molar ratio of Ag_3PO_4 to HA (0.15, 0.3, 0.6, and 1.8) were prepared *via* the identical procedure, and the corresponding final products were named as HA/N-CDs/Ag_3PO_4-a, HA/N-CDs/Ag_3PO_4-b, HA/N-CDs/Ag_3PO_4-c, and HA/N-CDs/Ag_3PO_4-d. For comparison, HA/Ag_3PO_4 with 0.15 of theoretical molar ratio of Ag_3PO_4 to HA was synthesized using the identical procedure. The synthesized process of HA/N-CDs/Ag_3PO_4 is shown in Fig. 1.

2.2 Characterization

The structure and crystallinity of the samples were examined *via* X-ray diffraction (XRD) using CuK_α radiation at 40 kV and 30 mA. The microstructures and morphologies were determined by transmission electron microscopy (TEM) and high-resolution TEM (HRTEM) coupled with energy dispersive X-ray spectroscopy (EDS). The compositions and chemical states of the samples were analyzed using X-ray photoelectron spectroscopy (XPS) (Thermo ESCALAB 250) equipped with a multichannel detector. The UV-Vis absorption spectra were recorded using a Shimadzu UV-2550 spectrophotometer in the wavelength range of 200–800 nm. The electron spin resonance (ESR) signals of hydroxyl radical ($^{\bullet}OH$) and superoxide radical ($^{\bullet}O_2^-$) trapped by DMPO were measured by a Bruker model E500 spectrometer.

The photocatalytic performance of the prepared samples was evaluated by the photocatalytic degradation of MB aqueous solution under visible-light irradiation at ambient temperature. 0.04 g photocatalyst was suspended in 40 mL of MB aqueous solution (20 mg L^{-1}). The mixed solution was treated by ultrasonication for 10 min, and then stirred under the dark condition for 1 h to ensure the adsorption–desorption equilibrium before visible-light irradiation. The reaction solution was subsequently positioned 20 cm away from the reactor and irradiated under continuous stirring. A 300 W Xe arc lamp with an UV-cutoff filter ($\lambda < 420$ nm) was used as a visible light source. After irradiation for some time, about 2 mL of the reaction solution was withdrawn and centrifuged. The concentration of MB was determined by measuring the absorbance peak at 664 nm *via* a UV-Vis spectrophotometer. For comparison, blank experiment was also performed in the absence of photocatalyst.

To investigate the stability of heterostructured HA/N-CDs/Ag_3PO_4 composite, consecutive three times recycling experiments were carried out as follows. After one cycle, the HA/N-CDs/Ag_3PO_4 powders were treated with ultrasonication, collected by centrifugation, and washed by distilled water three times. After dried at 60 °C for 12 h in a vacuum oven, the recycled HA/N-CDs/Ag_3PO_4 powders were collected and reused in the next cycle.

3. Results and discussion

3.1 Characterization of prepared photocatalysts

Fig. 2 shows the XRD patterns of as-prepared pure HA, HA/N-CDs and HA/N-CDs/Ag_3PO_4. It is seen that all the diffraction

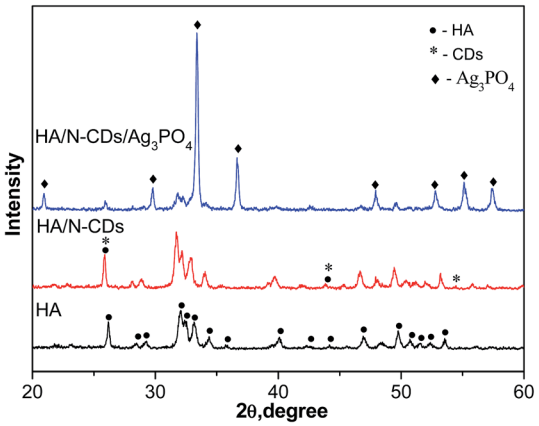

Fig. 2 XRD patterns of pure HA, HA/N-CDs and HA/N-CDs/Ag_3PO_4.

peaks of obtained pure HA could be well indexed to the pattern of HA (JCPDS, 009-0432). The XRD pattern of HA/N-CDs was similar with that of pure HA, except that the peak at 26° became stronger due to the characteristic peak of graphite at the same angle, indicating CDs were coupled with HA. For HA/N-CDs/Ag_3PO_4, it can be seen that some additional peaks were detected which are indexed to Ag_3PO_4 (JCPDS, 006-0505), revealing that Ag_3PO_4 formed after *in situ* ion-exchange reaction with HA and did not change HA structure.

Fig. 3 shows the TEM images of HA, N-CDs, Ag_3PO_4 and HA/N-CDs/Ag_3PO_4. It is seen that HA exhibited rod-like morphology (Fig. 3A). N-CDs were dispersed uniformly on TEM grid (Fig. 3B) and presented a round shape with diameters ranging from 1 to 5 nm. And nanosized Ag_3PO_4 particles were observed (Fig. 3C). For HA/N-CDs/Ag_3PO_4, it can be seen from Fig. 3D that Ag_3PO_4 particles with size of 5–10 nm dispersed on the surface of HA. The size of Ag_3PO_4 particles was smaller than bare Ag_3PO_4, implying the *in situ* ion-exchange method could effectively reduce the size of Ag_3PO_4 particles. As can be seen from the corresponding HRTEM image (Fig. 3E), CDs were found. In addition, the HRTEM image clearly displays the lattice spacing of 0.279 nm, 0.267 nm and 0.204 nm, corresponding to the HA (112) plane, Ag_3PO_4 (210) plane and CDs (101) plane. The EDS pattern of HA/N-CDs/Ag_3PO_4 was also shown in Fig. 3F. The characteristic signals of Ca, P and O were derived from HA, and signals of Ag were derived from Ag_3PO_4. These results suggested that the HA/N-CDs/Ag_3PO_4 composite was successfully obtained.

The XPS was also evaluated to further investigate the elemental compositions and chemical states of the samples. Fig. 4A shows the high-resolution C1s XPS spectra of HA/N-CDs/Ag_3PO_4-a in comparison to HA/Ag_3PO_4 (with the same theoretical molar ratio (0.15) of Ag_3PO_4 to HA). It is seen that the main C1s peaks at about 284.8 eV and 288.8 eV for HA/Ag_3PO_4 were observed although no CDs were added. This is because CO_2 inevitably was adsorbed and incorporated into the HA structure during the preparation. After the introduction of CDs, it was observed that the two peaks for HA/N-CDs/Ag_3PO_4 became stronger. Fig. 4B shows the high-resolution XPS spectra of O1s. It can be seen that the peak at 531 eV of HA/N-CDs/Ag_3PO_4-a is stronger than that of HA/Ag_3PO_4. This is also attributed to the presence of CDs which possess a certain content of O-containing groups such as C–O and C=O.[29] The high-resolution XPS spectra of Ag3d (Fig. 4C) show the binding energy of the $Ag3d_{5/2}$ and $Ag3d_{3/2}$ peaks at 368 eV and 374 eV. It is interesting to found that the two peaks for HA/N-CDs/Ag_3PO_4-a became weaker than that of HA/Ag_3PO_4. The reduction of the peak intensity was associated with the CDs shell on the surface of Ag_3PO_4 that obstructed the detection. These above results fully confirmed that the HA/N-CDs/Ag_3PO_4 composite was well achieved.

Fig. 5 shows the UV-Vis absorption spectra of HA/N-CDs, HA/Ag_3PO_4 and HA/N-CDs/Ag_3PO_4-a. It is seen that the absorption intensity of HA/N-CDs was weakest. For HA/Ag_3PO_4 obtained *via* ion-exchange method, it was observed a red shift in the absorption edge and the increased absorption intensity. This is attributed to the narrow band gap of Ag_3PO_4 (2.5 eV), leading to a wider absorption in the visible-light region. Compared to HA/N-CDs and HA/Ag_3PO_4, the visible-light absorption of HA/N-CDs/Ag_3PO_4-a was further enhanced. The stronger absorption is beneficial for improving photocatalytic performance.

3.2 Photocatalytic performance and mechanisms

3.2.1 Photocatalytic performance. The photocatalytic activities of the as-prepared photocatalysts were evaluated by the photocatalytic degradation of MB under visible-light irradiation, as shown in Fig. 6. In addition, control experiment of the degradation of MB was tested under visible-light irradiation in the absence of the photocatalyst, which showed that MB was not degraded. For comparison, the photocatalytic performance of HA/N-CDs and HA/Ag_3PO_4 was also tested under identical experimental conditions.

It is seen that 50 min was taken to degrade 90% of MB for HA/N-CDs, which was in agreement with our previous result.[32] And 25 min was taken to degrade about 92% of MB for HA/Ag_3PO_4. The improvement of the photocatalytic activity for HA/Ag_3PO_4 was associated with the good absorption of Ag_3PO_4 in the visible-light region (Fig. 5). It should be noted here that the photocatalytic activity of HA/Ag_3PO_4 in the present study was much better than that reported by Hong *et al.*[13] (68% of MB was degraded after 20 min irradiation), which could be attributed to the characteristics of HA support. The obtained HA in our study had high purity and crystallization (Fig. 2). In particular, the rod-like nanosized HA exhibited no aggregation (Fig. 3A). The good dispersibility of HA could be favorable for the synthesis of uniform Ag_3PO_4 on its surface. Compared with HA/N-CDs and HA/Ag_3PO_4, a significant result observed in this study was that HA/N-CDs/Ag_3PO_4-a exhibited the highest photocatalytic activity, and 98% of MB was degraded after 20 min irradiation. Simultaneously, the characteristic absorption of MB ($\lambda_{max} = 664$ nm) (inset in Fig. 6A) was observed to decrease with increasing the irradiation time, implying that MB decomposed.

To better investigate the photocatalytic performance of as-prepared samples, a kinetic study *via* using pseudo-first-order kinetics was evaluated, as shown in Fig. 6B. The degradation rate of MB on HA/N-CDs/Ag_3PO_4-a was calculated to 0.1782

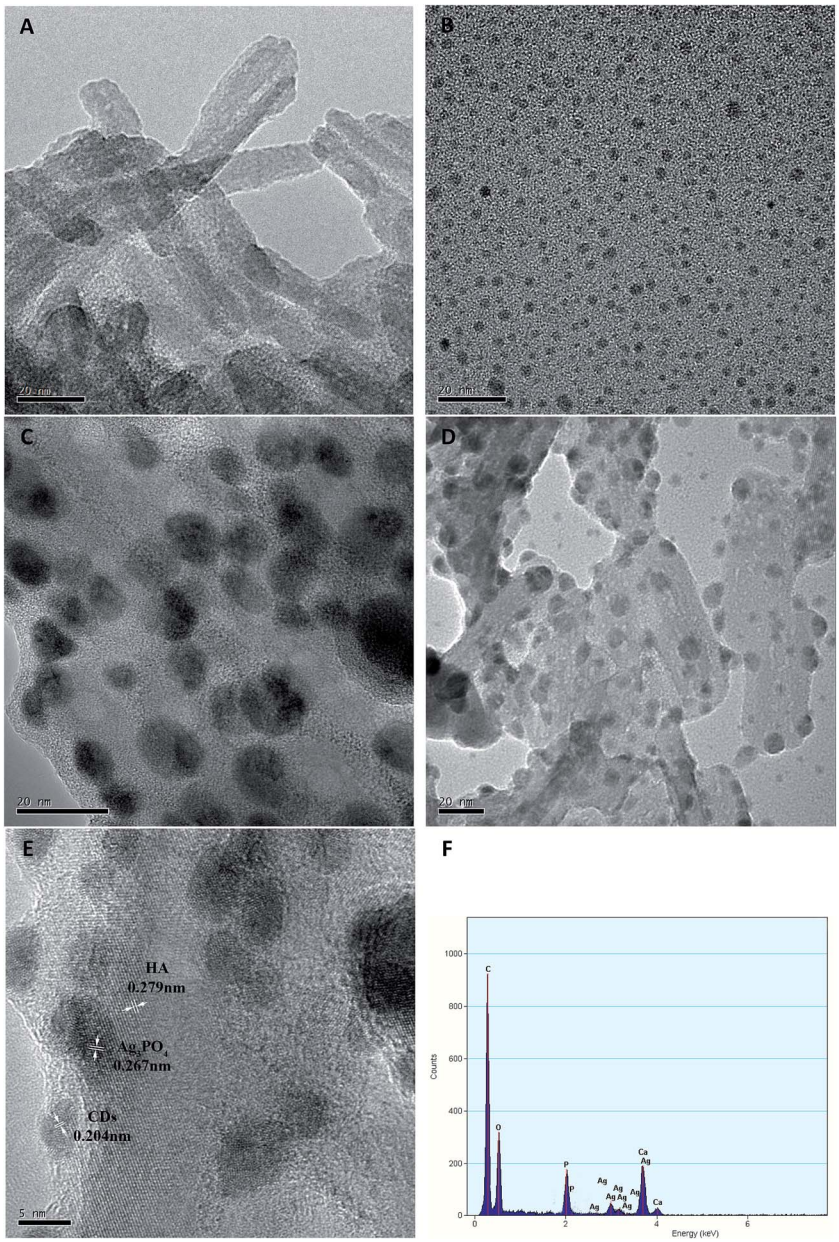

Fig. 3 TEM images (A–D) of HA, N-CDs, Ag_3PO_4, HA/N-CDs/Ag_3PO_4, HRTEM image (E) and EDS analysis (F) of HA/N-CDs/Ag_3PO_4.

min^{-1}, which was about 4.2 times of HA/N-CDs (0.04217 min^{-1}) and 1.8 times of HA/Ag_3PO_4 (0.09635 min^{-1}). The above results strongly suggested that the ternary HA/N-CDs/Ag_3PO_4 composite can be used as a new and effective visible-light-responsive photocatalyst.

3.2.2 Effects of silver loading amount on the photocatalytic performance. To better understand the photocatalytic behavior of HA/N-CDs/Ag_3PO_4, the composites with different silver loading amount were prepared by adding different $AgNO_3$. Fig. 7A shows the XRD pattern of HA/N-CDs/Ag_3PO_4-a, HA/N-CDs/Ag_3PO_4-b, HA/N-CDs/Ag_3PO_4-c, and HA/N-CDs/Ag_3PO_4-d. It is seen that four samples exhibited similar XRD patterns. With increasing the silver loading amount, the peak intensity of Ag_3PO_4 first increased and then decreased, while HA peaks almost disappeared. It is suggested that the content of Ag_3PO_4 on the HA surface increased. In addition, it was observed that the crystallization of HA/N-CDs/Ag_3PO_4 also increased first and then decreased with increasing the content of silver loading. The lower crystallization of HA/N-CDs/Ag_3PO_4-d might be attributed to the synthetic method of Ag_3PO_4. Further studies are needed. It should be noted here that the lower crystallization of Ag_3PO_4 is unstable which would have a negative effect on the photocatalytic activity.

Fig. 7B and C show the UV-Vis absorption spectra and photocatalytic activities of the samples. With the same trend as that of the XRD intensity, both the absorption in the whole visible-light and the photocatalytic performance increased first and then decreased with increasing the content of silver loading.

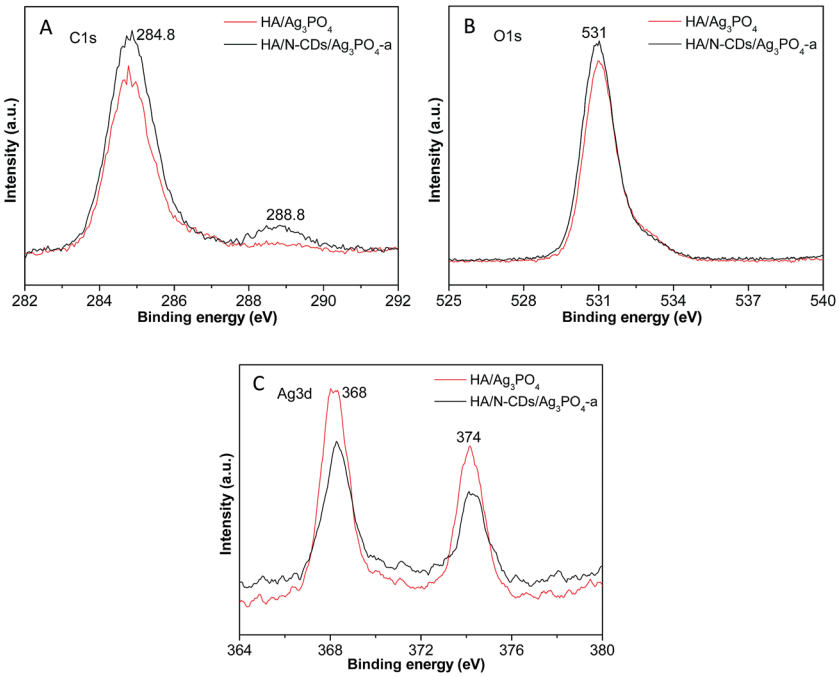

Fig. 4 XPS spectra of HA/Ag_3PO_4 and $HA/N\text{-}CDs/Ag_3PO_4$-a: (A) C1s, (B) O1s and (C) Ag3d.

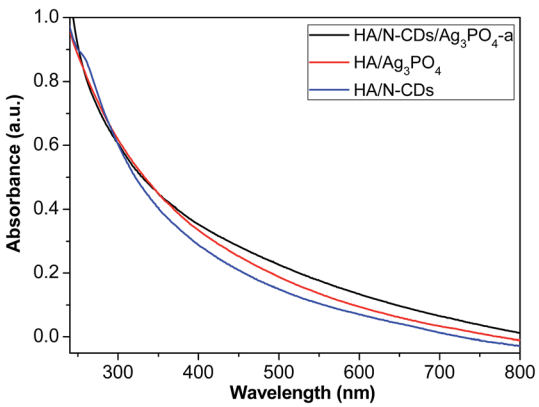

Fig. 5 UV/Vis absorption spectra of HA/N-CDs, HA/Ag_3PO_4 and $HA/N\text{-}CDs/Ag_3PO_4$-a.

$HA/N\text{-}CDs/Ag_3PO_4$-c exhibited the widest and strongest absorption and showed the highest photocatalytic activity. 98% of MB was degraded after 6 min irradiation. The characteristic absorption of MB (λ_{max} = 664 nm) (inset in Fig. 7C) almost disappeared after 6 min irradiation. Moreover, the decomposition rate of MB was also calculated, as shown in Fig. 7D. It is seen that the rate of $HA/N\text{-}CDs/Ag_3PO_4$-c reached the maximum value of 0.5850 min^{-1}.

These results demonstrated that further increase of silver loading amount ($HA/N\text{-}CDs/Ag_3PO_4$-d) resulted in the decrease of both the UV-Vis absorption and photocatalytic performance. This was related with two potential reasons. First, the photocorrosion of Ag_3PO_4 could happen due to its lower crystallization for $HA/N\text{-}CDs/Ag_3PO_4$-d, as revealed by XRD patterns (Fig. 7A). Second, CDs which played key role in protecting dissolution of Ag_3PO_4 were covered by the excess Ag_3PO_4. Therefore, further increase of the content of silver loading led to

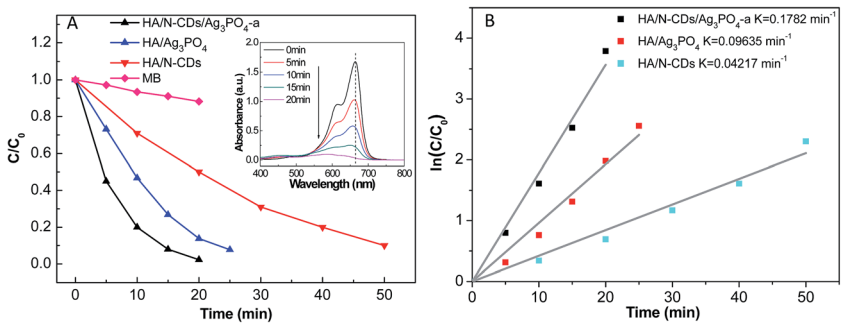

Fig. 6 (A) Photocatalytic activities of HA/N-CDs, HA/Ag_3PO_4 and $HA/N\text{-}CDs/Ag_3PO_4$-a for MB degradation under visible-light irradiation, and (B) plots of $\ln(C/C_0)$ *versus* irradiation time (t).

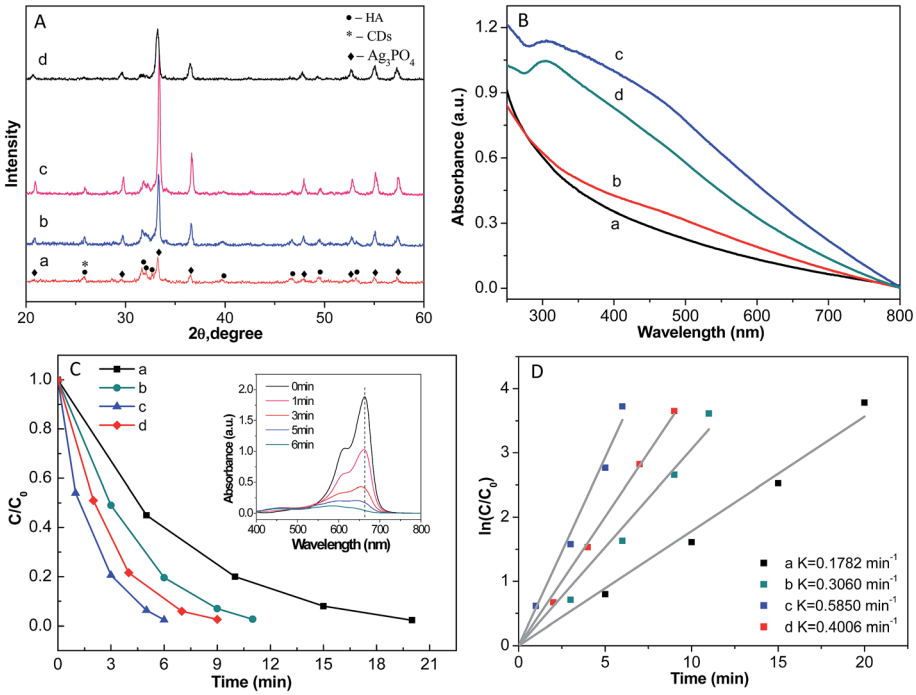

Fig. 7 (A) XRD patterns of HA/N-CDs/Ag_3PO_4 with different silver loading amount, (B) UV/Vis absorption spectra, (C) photocatalytic activities, and (D) plots of ln(C/C_0) *versus* irradiation time (t).

a decrease of both the absorption property and photocatalytic activity.

Furthermore, the stability of a photocatalyst is needed for its far-reaching applications. In this study, recycle experiments of MB degradation on the sample HA/N-CDs/Ag_3PO_4-c with the best photocatalytic performance was investigated and the corresponding result is shown in Fig. 8. It can be clearly seen that although the photocatalytic activity showed slight decrease, the degradation of MB was maintained at 95% after three repeated cycles, suggesting high stability of HA/N-CDs/Ag_3PO_4.

3.3 Photocatalytic mechanisms

It is necessary to develop efficient visible-light photocatalysts. Based above results, the HA/N-CDs/Ag_3PO_4 composite in the present study showed excellent photocatalytic activity and stability under visible-light irradiation. Possible photocatalytic mechanisms are proposed.

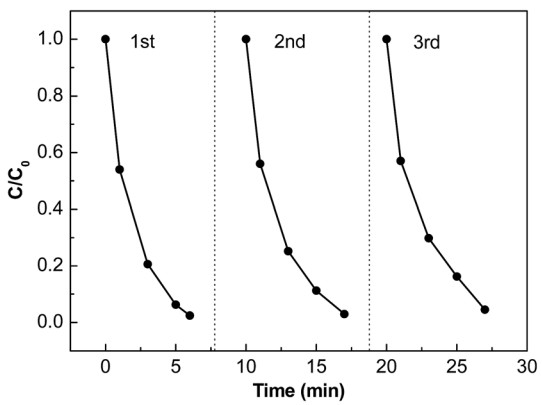

Fig. 8 Recycle experiments of MB degradation by HA/N-CDs/Ag_3PO_4-c.

First, the photocatalytic activity is inherently determined by its composition. Although Ag_3PO_4 is an efficient visible-light photocatalyst, it possesses certain solubility in aqueous solution and has relative larger particle size.[14] The two factors intrinsically weaken the photocatalytic activity. In this study, CDs dispersed on the surface of the composite that could effectively prevent the dissolution of Ag_3PO_4 so as to improve the photocatalytic activity and the stability of the composite. Moreover, CDs also possess the property of the broadband optical absorption. Therefore, compared with HA/N-CDs and HA/Ag_3PO_4, HA/N-CDs/Ag_3PO_4 composite exhibited a higher absorption intensity in the visible region (Fig. 5).

Second, the activity of a photocatalyst is also dependent on its microstructure. As revealed by the TEM results (Fig. 3), in this study, HA nanorods with tens of nanometers in length were obtained. CDs and Ag_3PO_4 were homogeneously distributed on the HA surface. The obtained strawberry-like structure could give a high surface area that can strengthen light harvesting. In addition, the size of Ag_3PO_4 was in the range of 5–10 nm, which is also beneficial for the enhanced photocatalytic activity. Importantly, the conjugation between HA and N-CDs was due to the interaction between hydroxyl on the surface of HA and surface groups of N-CDs,[32] which could lead to a good interfacial bonding. What is more, Ag_3PO_4 prepared *via in situ* ion-exchange method intrinsically had an appropriate bonding between HA. Therefore, a good connection between them was obtained, which could be the potential transfer channel of the photogenerated electrons and holes, giving rise to a reduction

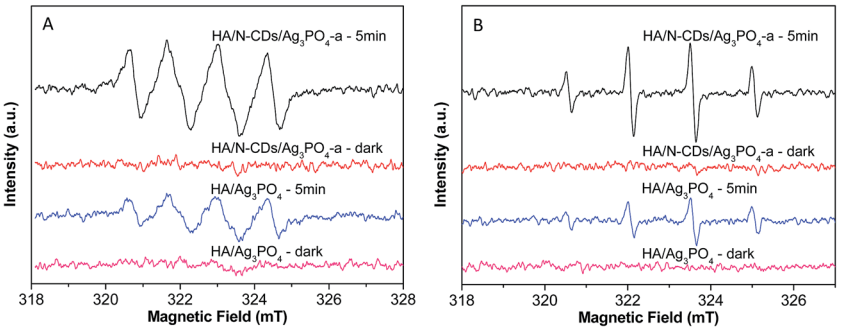

Fig. 9 ESR signals of HA/Ag_3PO_4 and $HA/N\text{-}CDs/Ag_3PO_4$-a: (A) $^{\bullet}O_2^-$ and (B) $^{\bullet}OH$.

of the recombination. So the photocatalytic performance of the ternary composite was remarkably improved.

Third, a key factor that affects the activity of the photocatalysts is the abundant surface active sites which depend on the separation and transfer of the photogenerated electrons (e^-) and holes (h^+). For Ag_3PO_4, the photogenerated electrons tend to reduce Ag^+ to Ag rather than form superoxide radical in the absence of electron acceptors since the potential of the conduction band (CB) is more positive than the reduction potential of O_2 (−0.33 eV *vs.* NHE).[14] However, the superoxide radicals ($^{\bullet}O_2^-$) are the important reactive species for decomposing organic molecules. In the present study, we examined the main oxidative centers ($^{\bullet}O_2^-$ and $^{\bullet}OH$) in the HA/Ag_3PO_4 and $HA/N\text{-}CDs/Ag_3PO_4$ composites by a spin trapping method, as shown in Fig. 9. As seen from the Fig. 9A, the peaks of the DMPO–$^{\bullet}O_2^-$ adducts for HA/Ag_3PO_4 were observed under visible light irradiation for 5 min, which was in agreement with the literature reported by Chai *et al.*[14] In comparison to HA/Ag_3PO_4, a significant result was observed that the ESR signal for $HA/N\text{-}CDs/Ag_3PO_4$ composite was much stronger, implying more $^{\bullet}O_2^-$ radicals were formed. For the ESR spectra of $^{\bullet}OH$ trapped by DMPO (Fig. 9B), it can also be seen that a much stronger ESR signal was produced on the $HA/N\text{-}CDs/Ag_3PO_4$ than on the HA/Ag_3PO_4, with the same trend as that of ESR spectra of $^{\bullet}O_2^-$. The results proved the formation of the more oxidizing active sites for the ternary composite in the photodegradation process. The more the active sites, the higher the photocatalytic degradation of organic molecules. The above results were well consistent with the photoactivity results (Fig. 6). This could be understood as follows.

Fig. 10 illustrates the separation and transfer behaviors of photogenerated electrons and holes of the ternary composite.

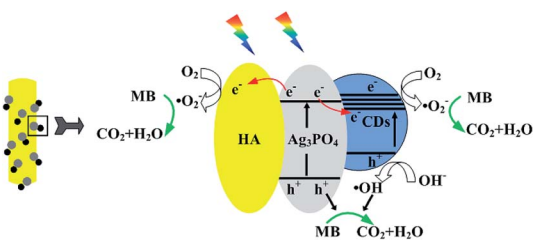

Fig. 10 Photocatalytic mechanisms for MB degradation by $HA/N\text{-}CDs/Ag_3PO_4$.

Under visible-light irradiation, photogenerated electrons and holes of Ag_3PO_4 and CDs were produced. It is known that CDs could act as both the electron acceptors and donors. As electron acceptors, they can trap photogenerated electrons from Ag_3PO_4, thus effectively suppressing the recombination of the photogenerated electron/hole pairs and impeding the photocorrosion of Ag_3PO_4. Meanwhile, the photogenerated electrons could also migrate to HA due to its storage property of electrons,[15] leading to the separation of electron–hole pairs. The electrons accumulated on CDs and HA could adsorb the O_2 in solution to form $^{\bullet}O_2^-$ (Fig. 9A), which could degrade the MB. The electrons that created the superoxide radicals resulted in another kind of significant oxidizing active sites of photogenerated holes. In addition, the higher quantity of holes (h^+) led to the increase of $^{\bullet}OH$ (Fig. 9B), which could significantly improve the photocatalytic activity. As a consequence, the heterostructured $HA/N\text{-}CDs/Ag_3PO_4$ photocatalyst exhibited excellent photocatalytic performance.

4. Conclusions

In summary, a new $HA/N\text{-}CDs/Ag_3PO_4$ photocatalyst has been successfully achieved *via* a cost-effective route. The photocatalytic performance was studied for the degradation of MB under visible light irradiation. The results showed that the heterostructured $HA/N\text{-}CDs/Ag_3PO_4$ composite can be used as a new and effective visible-light-responsive photocatalyst. An appropriate silver loading amount could make the composite exhibit the best photocatalytic activity and good structure stability. The remarkable photocatalytic performance and stability arised from the synergetic effects of the ternary components, which provided more active sites, suppressed the recombination of photoinduced electron–hole pairs, and impeded the photocorrosion and dissolution of formed Ag_3PO_4. It is expected that the $HA/N\text{-}CDs/Ag_3PO_4$ photocatalyst has promising application in the removal of organic materials.

Acknowledgements

The authors would like to thank the financial support by the National Natural Science Foundation of China (No. 51502270, U1510125). Q. Chang is also grateful for the financial support by Shanxi Province Science Foundation (201601D021059),

Program for the Young Academic Leaders and the Natural Science Foundation of North University of China.

References

1 D. M. Schultz and T. P. Yoon, *Science*, 2014, **343**, 1239176.
2 X. J. Lang, X. D. Chen and J. C. Zhao, *Chem. Soc. Rev.*, 2014, **43**, 473–486.
3 Y. Y. Bai, Y. Lu and J. K. Liu, *J. Hazard. Mater.*, 2016, **307**, 26–35.
4 C. T. Dinh, H. Yen, F. Kleitz and T. O. Do, *Angew. Chem., Int. Ed.*, 2014, **53**, 6618–6623.
5 S. Kumar, A. Baruah, S. Tonda, B. Kumar, V. Shanker and B. Sreedhar, *Nanoscale*, 2014, **6**, 4830–4842.
6 C. Han, N. Zhang and Y. J. Xu, *Nano Today*, 2016, **11**, 351–372.
7 W. Wang, M. O. Tade and Z. P. Shao, *Chem. Soc. Rev.*, 2015, **44**, 5371–5408.
8 S. Ghosh, N. A. Kouame, L. Ramos, S. Remita, A. Dazzi, A. Deniset-Besseau, P. Beaunier, F. Goubard, P. H. Aubert and H. Remita, *Nat. Mater.*, 2015, **14**, 505–511.
9 M. Sadat-Shojai, M. T. Khorasani, E. Dinpanah-Khoshdargi and A. Jamshidi, *Acta Biomater.*, 2013, **9**, 7591–7621.
10 Z. Boukha, J. Gonzalez-Prior, B. de Rivas, J. R. Gonzalez-Velasco, R. Lopez-Fonseca and J. I. Gutierrez-Ortiz, *Appl. Catal., B*, 2016, **190**, 125–136.
11 P. Zhang, T. B. Wu, T. Jiang, W. T. Wang, H. Z. Liu, H. L. Fan, Z. F. Zhang and B. X. Han, *Green Chem.*, 2013, **15**, 152–159.
12 J. Xie, X. C. Meng, Z. Zhou, P. Li, L. Yao, L. Bian, X. R. Gao and Y. Wei, *Mater. Lett.*, 2013, **110**, 57–60.
13 X. Hong, X. Wu, Q. Zhang, M. Xiao, G. Yang, M. Qiu and G. Han, *Appl. Surf. Sci.*, 2012, **258**, 4801–4805.
14 Y. Y. Chai, J. Ding, L. Wang, Q. Q. Liu, J. Ren and W. L. Dai, *Appl. Catal., B*, 2015, **179**, 29–36.
15 L. L. Zhang, Q. Tong, X. Y. Zhang, Y. Lu, J. K. Liu, J. J. Wang and X. H. Yang, *Mater. Technol.*, 2014, **29**, A9–A13.
16 L. Dai, D. W. Chang, J. B. Baek and W. Lu, *Small*, 2012, **8**, 1130–1166.
17 F. Yuan, S. Li, Z. Fan, X. Meng, L. Fan and S. Yang, *Nano Today*, 2016, **11**, 565–586.
18 L. Cao, S. Sahu, P. Anilkumar, C. E. Bunker, J. Xu, K. A. Fernando, P. Wang, E. A. Guliants, K. N. Tackett and Y. P. Sun, *J. Am. Chem. Soc.*, 2011, **133**, 4754–4757.
19 A. Tyagi, K. M. Tripathi, N. Singh, S. Choudhary and R. K. Gupta, *RSC Adv.*, 2016, **6**, 72423–72432.
20 Z. J. Zhang, T. T. Zheng, X. M. Li, J. Y. Xu and H. B. Zeng, *Part. Part. Syst. Charact.*, 2016, **33**, 457–472.
21 Y. Q. Zhang, D. K. Ma, Y. G. Zhang, W. Chen and S. M. Huang, *Nano Energy*, 2013, **2**, 545–552.
22 H. C. Zhang, H. Huang, H. Ming, H. Li, L. L. Zhang, Y. Liu and Z. H. Kang, *J. Mater. Chem.*, 2012, **22**, 10501–10506.
23 R. Liu, H. Huang, H. Li, Y. Liu, J. Zhong, Y. Li, S. Zhang and Z. Kang, *ACS Catal.*, 2014, **4**, 328–336.
24 J. Di, J. Xia, Y. Ge, H. Li, H. Ji, H. Xu, Q. Zhang, H. Li and M. Li, *Appl. Catal., B*, 2015, **168–169**, 51–61.
25 J. H. Park, F. Raza, S. J. Jeon, D. Yim, H. I. Kim, T. W. Kang and J. H. Kim, *J. Mater. Chem. A*, 2016, **4**, 14796–14803.
26 S. L. Hu, R. X. Tian, L. L. Wu, Q. Zhao, J. L. Yang, J. Liu and S. R. Cao, *Chem.–Asian J.*, 2013, **8**, 1035–1041.
27 S. L. Hu, Y. L. Ding, Q. Chang, J. L. Yang and K. Lin, *Appl. Surf. Sci.*, 2015, **355**, 774–777.
28 S. L. Hu, Q. Chang, K. Lin and J. L. Yang, *Carbon*, 2016, **105**, 484–489.
29 S. L. Hu, *Chem. Rec.*, 2016, **16**, 219–230.
30 S. L. Hu, Z. J. Wei, Q. Chang, A. Trinchi and J. L. Yang, *Appl. Surf. Sci.*, 2016, **378**, 402–407.
31 S. L. Hu, W. Y. Zhang, Q. Chang, J. L. Yang and K. Lin, *Carbon*, 2016, **103**, 391–393.
32 Q. Chang, K. K. Li, S. L. Hu, Y. G. Dong and J. L. Yang, *Mater. Lett.*, 2016, **175**, 44–47.
33 U. Sulaeman, F. Febiyanto, S. Yin and T. Sato, *Catal. Commun.*, 2016, **85**, 22–25.
34 W. S. Wang, H. Du, R. X. Wang, T. Wen and A. W. Xu, *Nanoscale*, 2013, **5**, 3315–3321.
35 Q. Xiang, D. Lang, T. Shen and F. Liu, *Appl. Catal., B*, 2015, **162**, 196–203.
36 X. F. Yang, H. Y. Cui, Y. Li, J. L. Qin, R. X. Zhang and H. Tang, *ACS Catal.*, 2013, **3**, 363–369.
37 X. F. Yang, J. L. Qin, Y. Jiang, R. Li, Y. Li and H. Tang, *RSC Adv.*, 2014, **4**, 18627–18636.
38 X. F. Yang, H. Tang, J. Xu, M. Antonietti and M. Shalom, *ChemSusChem*, 2015, **8**, 1350–1358.
39 X. F. Yang, J. L. Qin, Y. Jiang, K. M. Chen, X. H. Yan, D. Zhang, R. Li and H. Tang, *Appl. Catal., B*, 2015, **166**, 231–240.
40 X. F. Yang, Z. P. Chen, J. S. Xu, H. Tang, K. M. Chen and Y. Jiang, *ACS Appl. Mater. Interfaces*, 2015, **7**, 15285–15293.

